Fuel Processing Technology 90 (2009) 360–366

Contents lists available at ScienceDirect

Fuel Processing Technology

journal homepage: www.elsevier.com/locate/fuproc

Experimental investigation of a packed-bed solar reactor for the steam-gasification of carbonaceous feedstocks

Nicolas Piatkowski [a,1], Christian Wieckert [b,2], Aldo Steinfeld [a,b,*]

[a] Department of Mechanical and Process Engineering, ETH Zurich, 8092 Zurich, Switzerland
[b] Solar Technology Laboratory, Paul Scherrer Institute, 5232 Villigen PSI, Switzerland

ARTICLE INFO

Article history:
Received 17 June 2008
Received in revised form 13 October 2008
Accepted 14 October 2008

Keywords:
Solar
Gasification
Syngas
Hydrogen
Packed bed

ABSTRACT

Steam-gasification of coal, biomass, and carbonaceous waste feedstocks for syngas production is performed using concentrated solar energy as the source of high-temperature process heat. The solar reactor consists of two cavities separated by a SiC-coated graphite plate, with the upper one serving as the radiative absorber and the lower one containing the reacting packed bed that shrinks as the reaction progresses. The carbonaceous feedstocks tested were industrial and sewage sludges, scrap tire powder, fluff, South African coal, and beech charcoal, and are characterized by having a wide range of volatile, ash, and fixed carbon contents, elemental compositions, and physical properties. A 5 kW solar reactor prototype, subjected to radiative flux concentrations up to 2953 suns and operated at temperatures up to 1490 K, yielded high-quality syngas of typical molar ratios $H_2/CO=1.5$ and $CO_2/CO=0.2$, and with a calorific content up to 30% upgraded over that of the input feedstock. Solar-to-chemical energy conversion efficiencies varied between 17.3% and 29%. Pyrolysis was evident through the evolution of higher gaseous hydrocarbons and liquid tars during heating of the packed bed. The engineering design, fabrication, and testing of the solar reactor are described.

1. Introduction

Solar steam-gasification of carbonaceous materials makes use of concentrated solar energy to convert solid feedstocks such as coal, biomass, or carbon-containing wastes into high-quality synthesis gas (syngas)—mainly H_2 and CO—applicable for power generation in efficient combined cycles and fuel cells, or for Fischer–Tropsch processing to liquid fuels. Conventional autothermal gasification requires a portion of the introduced feedstock to be combusted with pure O_2 to supply high-temperature process heat for the endothermic gasification reaction. The impact on the operation of conventional gasifiers is seen by comparing the endothermic steam-gasification reaction enthalpy with the *LHV* of the input feedstock. For example, 12 MJ/kg are required to steam-gasify a typical bituminous coal at 1200 K while the *LHV* of this coal is 34 MJ/kg [1]. Therefore, an autothermal coal gasifier running with bituminous coal requires that at least 35% of the introduced coal mass be burned uniquely to power the gasification reaction. Obviously, this technique has poor feedstock utilization and contaminates the syngas with combustion products (e.g., CO_2, SO_x). In contrast, solar-driven steam-gasification is free of nearly all combustion byproducts. Furthermore, the syngas produced has a lower CO_2 intensity because its calorific value is solar-upgraded over that of the original feedstock by an amount equal to the enthalpy change of the reaction. A 2nd-law analysis indicated that Brayton–Rankine combined power cycles running on solar-made syngas stemming from coal can double the specific electric output per unit mass of coal and, consequently, avoid half the specific CO_2 emissions of conventional coal-fired generation plants [1]. Solar thermochemical gasification of carbonaceous feedstocks is ultimately a means of chemically storing intermittent solar energy in a dispatchable form. Furthermore, it has the potential of becoming economically more favorable than conventional gasification. The total costs for a rudimentary solar coal gasifier were compared against a Lurgi autothermal gasifier and estimated to be 13% lower per unit of produced syngas [2]. The two determining factors were found to be the high cost of producing a stream of pure oxygen from air—due to the high energy intensity and infrastructure of the separation process—as well as a 43% higher coal consumption for the Lurgi gasifier against the solar gasifier per unit of produced syngas [2].

* Corresponding author. Department of Mechanical and Process Engineering, ETH Zurich, 8092 Zurich, Switzerland. Tel.: +41 44 6327929; fax: +41 44 6321065.
E-mail addresses: nicolapi@ethz.ch (N. Piatkowski), christian.wieckert@psi.ch (C. Wieckert), aldo.steinfeld@eth.ch (A. Steinfeld).
[1] Tel.: +41 44 632 34 47.
[2] Tel.: +41 56 310 44 07.

0378-3820/$ – see front matter
doi:10.1016/j.fuproc.2008.10.007

Table 1
Ultimate and proximate analyses and packed bed properties of carbonaceous feedstocks considered for steam-gasification

Feedstock	Industrial sludge	Sewage sludge	Scrap tire powder	Fluff	South African coal	Beech charcoal
Ultimate analysis (daf)						
C (wt.%)	46.2	27.1	82.2	51.3	64.5	82.3
H (wt.%)	5.12	4.0	7.3	6.9	3.5	3.21
O (wt.%)	<25	17.3	3.6	22.5	6.0	7.0
N (wt.%)	<2	3.5	0.39	0.64	1.5	0.38
S (wt.%)	0.59	0.83	1.9	0.74	0.42	0.05
Proximate analysis						
Ash (wt.%)	20	33.4	4.5	6.07	14.1	2.4
Volatile (wt.%)	62.2	51.9	67.5	82.5	21	17.3
Water (wt.%)	5.5	7.2	1.0	1	8.9	4
C-fix (wt.%)	12.4	7.4	27	10.4	55.9	80.3
$LHV_{feedstock}$ (kJ/kg)	19,305	10,288	35,515	24,868	24,973	32,127
Packed bed and particle properties						
Particle size range (mm)	10–30	0.1–3	0.1–2.5	5–30	8	2
Particle form	Irregular chunks	Regular particles	Regular particles	Irregular flakes	Regular chunks	Regular flakes
Bed porosity	0.4	0.3	0.28	0.7	0.46	0.43

Solar gasification of petroleum coke and coal was studied in directly irradiated fluidized-bed and vortex-flow solar reactors [3–8]. Direct irradiation of these particle suspensions was found to be an effective means of heat transfer directly to the reaction site, leading to extremely fast heating rates (~1000 K/s) and enhanced kinetics [8]. However, the transparent quartz window needed for the optical access of concentrated solar radiation becomes a troublesome, critical component under high pressures and severe atmospheres. The large volume flow rates of inert carrier gases or excess steam necessary for fluidization and for protecting the window displace syngas, decreasing production and energy conversion efficiency [9]. Additionally, effective fluidization requires small particle sizes (<5 mm) and narrow particle size distributions, making particle suspension reactors ill-suited to highly variable feedstocks and more costly due to extra feedstock handling operations [9]. A number of exploratory studies investigated solar gasification of coal, oil shales, and biomass in packed-bed reactors [10,11]. These types of reactors sought to mimic the operation of Lurgi class autothermal packed-bed coal gasifiers which operate with a counter-flow of a steam/oxygen mixture and coal, establishing a temperature profile that progressively dries, devolatizes, carbonizes, and gasifies the feedstock as it moves within the chamber [9,10]. Conventional steam-gasification of carbonaceous wastes has been studied in the laboratory as well as in large-scale industrial waste-to-energy plants [12–15]. For a variety of wastes, fuel-to-electric efficiencies were improved by up to 50% compared to direct waste combustion with 75–85% of the introduced feedstock energy content captured in the syngas [13].

This paper presents the experimental investigation of the steam-gasification of coal, biomass, and carbonaceous waste feedstocks in a solar-driven packed-bed reactor. The solar reactor design and its installation are presented in detail followed by the experimental results obtained from tests under concentrated thermal radiation.

2. Investigated carbonaceous feedstocks

The feedstocks considered for steam-gasification represent a wide range of physical and chemical properties which are shown in Table 1.

Industrial sludge is a carbonaceous waste consisting of paints, solvents, inks, glues, and oily residues. Sewage sludge, also a carbonaceous waste, is the residue from municipal waste water treatment. The water contents given in Table 1 refer to water remaining in the feedstocks after dewatering and prior to introduction into the reactor. Normally a waste, scrap tire powder is an industrial product

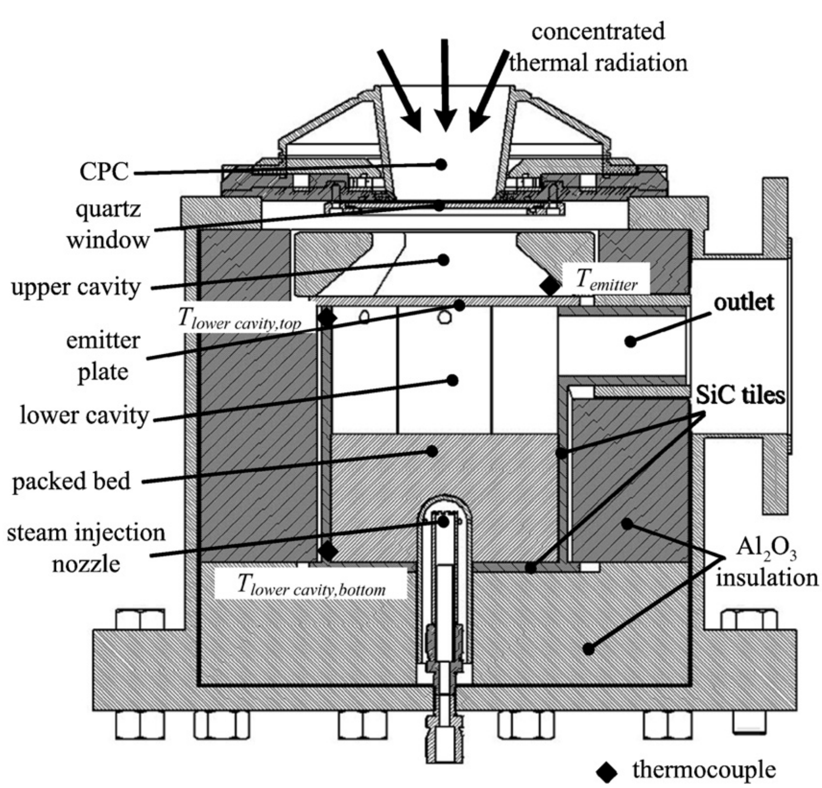

Fig. 1. Section view of the packed-bed solar reactor, featuring two cavities separated by an emitter plate, with the upper one serving as the radiative absorber and the lower one containing the reacting packed bed that shrinks as the reaction progresses.

Table 2
Operational parameters for the steam-gasification of carbonaceous feedstocks

Feedstock	Industrial sludge	Sewage sludge	Scrap tire powder	Fluff	South African coal	Beech charcoal
Packed-bed initial height (cm)	11	9.2	5.0	13.9	6.8	8.2
Packed-bed initial mass (kg)	0.550	0.802	0.288	0.629	0.67	0.335
Maximum solar concentration at aperture (suns)	2531	2953	2530	2652	2352	1960
Water vapor concentration (%)	0–76	0–65	0–83	0–65	0–70	0–82

due to milling and the removal of inert materials. Fluff is a highly heterogeneous waste consisting of synthetic textiles, paper, and shredded plastics. South African coal is a lower rank lignite used commonly as a fuel for steam-based power generation. Beech charcoal is an industrially made homogenous biomass feedstock. The four waste feedstocks have large volatile and low fixed carbon contents—characteristics which support the release of volatiles and tars but are less favorable for steam-gasification which takes place in a temperature range above that normally attributed to devolatilization. Feedstocks with significant residual water contents such as sewage sludge and South African coal can be expected to support steam-gasification reactions during drying in the reactor without steam addition. High inert material contents lead to low feedstock calorific values, as demonstrated by the ash content of sewage sludge and the correspondingly low $LHV_{\mathrm{feedstock}}$. Additionally the inert ash, due to low emissivity, has important consequences for radiative heat transfer to the packed bed as reactable material is depleted. Heat transfer by conduction in porous packed beds is generally poor; however, high porosities as in the case of fluff support high-temperature radiative heat transfer within the packed bed [16].

3. Solar reactor configuration and experimental set-up

The solar reactor is schematically shown in Fig. 1. It is specifically designed for beam-down incident solar radiation as obtained through a Cassegrain optical configuration that makes use of a hyperbolic reflector at the top of a solar tower to redirect sunlight collected by a heliostat field to a receiver located at ground level [17]. For large-scale reactor installations involving solid reactants (>250 kW), the beam-down solar tower is technically favorable considering structural limitations, feedstock/steam feeding, and off-gas handling. The solar reactor configuration features two cavities in series. The upper cavity functions as the solar absorber and contains a small windowed opening—the aperture—to accept concentrated solar radiation. The lower cavity functions as the reaction chamber and contains the packed bed on top of the steam injector. An emitter plate separates the two cavities. A 3D compound parabolic concentrator (CPC) is incorporated at the reactor's aperture to further augment the incident solar flux before passing it through a quartz window into the upper cavity. Thus, the emitter plate is directly irradiated and acts as solar absorber and radiant emitter to the lower cavity. Its main purpose is to eliminate contact between the quartz window and the reactants/products, preventing deposition of particles or condensable gases and ensuring a clean window during operation. It further provides uniform heating of the bed through re-radiation. The upper cavity also serves as a thermal shock absorber; a desired property given the intermittent nature of concentrated solar radiation. The reactor is operated in batch mode, with the packed bed shrinking as the gasification reaction progresses. This reactor concept was designed along the guidelines for “2-cavity” type solar reactors [18], which have been successfully applied to the carbothermal reduction of ZnO and for the detoxification of solid wastes [19–21]. This arrangement enables the reactor to receive a wide range of particle sizes and forms.

A 5 kW reactor prototype was fabricated with an upper cavity containing a 6.5 cm-diameter aperture and a 14.3 cm-diameter, 16 cm-height lower cylindrical cavity filled to varying depths for each feedstock, as listed in Table 2. The emitter plate was made of SiC-coated graphite. The upper cavity was sealed by a 3 mm-thick fused quartz window located at the aperture and purged with a 2 l_N/min Argon flow. Future reactor concepts will aim at eliminating the quartz window by sealing with the emitter plate. The lower cavity was lined with 6 mm-thick SiC tiles and with 70 mm-thick Al_2O_3–SiO_2 insulation. Due to the relatively high thermal conductivity of the SiC tiles (~25 W/mK), heat is transferred to the deeper regions of the

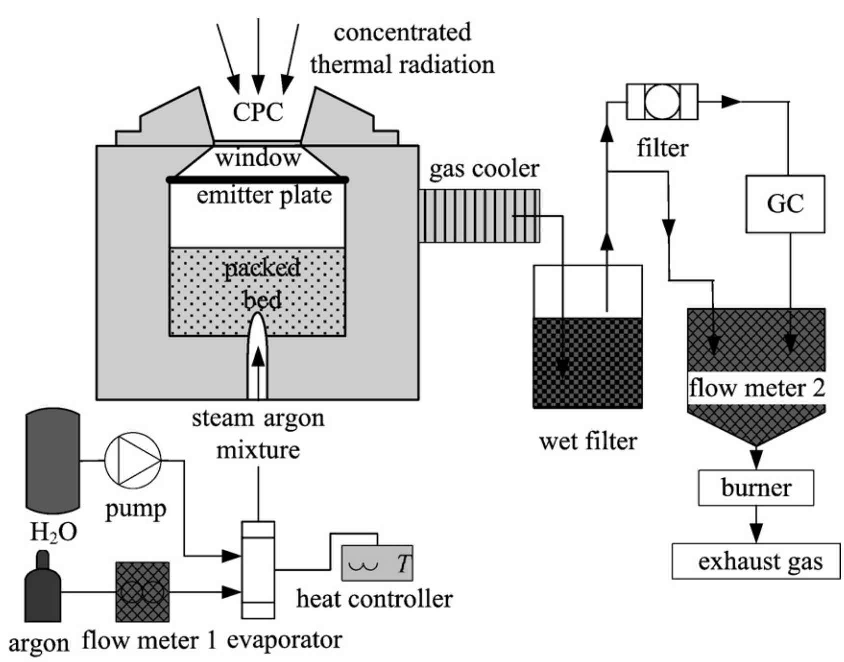

Fig. 2. Scheme of the solar reactor experimental set-up and associated peripheral devices as used in the High-Flux Solar Simulator.

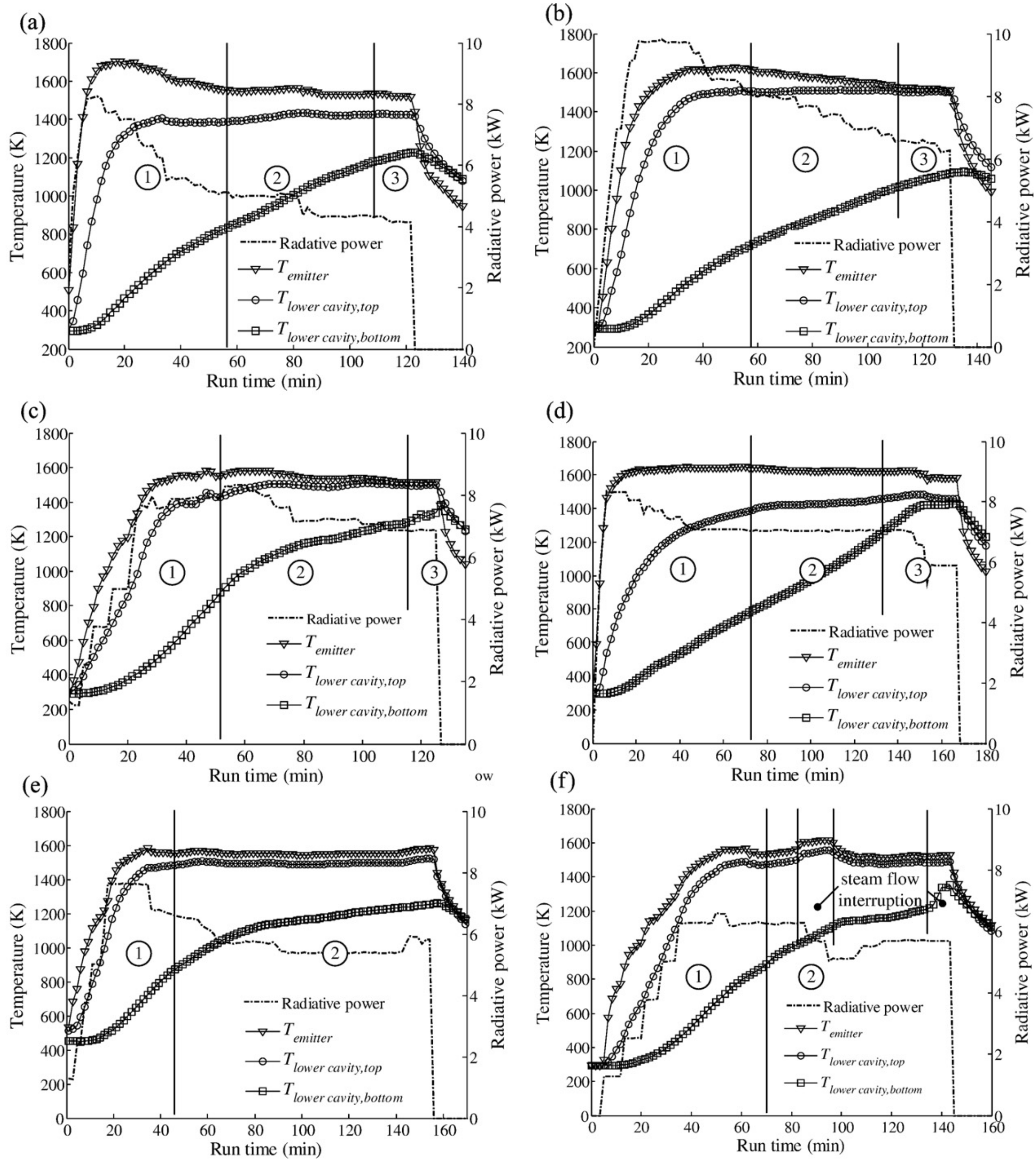

Fig. 3. Experimentally measured temperatures in the solar reactor and radiative power input through the reactor's aperture during the solar steam-gasification of: (a) industrial sludge, (b) sewage sludge, (c) scrap tire powder, (d) fluff, (e) South African coal, and (f) beech charcoal.

packed bed by conduction along the length of the tiles [22]. A steam–argon mixture at 400 K with liquid water flow rates up to 8 ml/min and an Ar flow rate of 2 l_N/min[3] was injected through 7 injection nozzles elevated 2.5 cm above the floor of the lower cavity. Product gases exited through a lateral outlet port where they underwent initial cooling down to 500 K and flowed across a wet filter to remove solid matter and accomplish the final cooling to ambient temperature. Gas composition was analyzed by gas chromatography (Agilent High Speed Micro GC G2890A, equipped with molecular sieve 5A and HaySep A capillary columns) with a sampling period of 145 s. All product gases were flared. Temperatures were measured at the top $T_{\text{lower cavity, top}}$ and bottom $T_{\text{lower cavity, bottom}}$ of the lower cavity with type-K thermocouples, and at the upper surface of the emitter plate T_{emitter} with a type-S thermocouple, as indicated in Fig. 1. The lower cavity thermocouples were mounted on the outer surface of the SiC walls to protect them from direct steam and ash exposure. Experimentation was carried out at PSI's High-Flux Solar Simulator (HFSS): an array of 10 Xenon arcs, close-coupled to ellipsoidal reflectors, which can simulate the radiative heat transfer characteristics of highly concentrating solar systems [23]. Radiative fluxes incident into the reactor were measured optically with a calibrated CCD camera on a water-cooled Al_2O_3-plasma coated Lambertian target. The maximum

[3] l_N means liters at normal conditions; mass flow rates are calculated at 273 K and 1 bar.

radiative flux at the reactor's aperture was equivalent to a solar concentration ratio of 2953 suns (1 sun = 1 kW/m^2). Fig. 2 shows the solar reactor set-up with associated peripheral devices as used in the HFSS.

4. Experimental results and discussion

The variation of temperatures for the three thermocouple locations (see Fig. 1) and radiative power input through the reactor's aperture during representative solar experimental runs are shown in Fig. 3 for the six carbonaceous feedstocks undergoing steam-gasification. Up to 7 Xe-arcs of the HFSS were used and ignited in sequence at 1–7 min intervals. With increasing radiative power through the aperture, T_{emitter} rose rapidly and stabilized at various levels due to the thermal inertia of the double cavity configuration. A fast increase in radiative power with a 1-minute arc ignition interval, as in the case of industrial sludge (Fig. 3a), produced a peak value of T_{emitter} at 1700 K, whereas a 7-minute arc ignition interval, as in the case of beech charcoal (Fig. 3f), produced a T_{emitter} maximum value of 1550 K. $T_{\mathrm{lower\ cavity,\ top}}$ followed T_{emitter} and the two temperatures converged over the course of the runs. It was shown through reactor modeling that $T_{\mathrm{lower\ cavity,\ top}}$ may be used to estimate the temperature on the bed top surface at the early stages of the experiment due to similar radiative view factors and surface properties [22]. $T_{\mathrm{lower\ cavity,\ bottom}}$ increased slowly due to the poor heat transfer within the packed bed and despite the additional heat delivered through conduction in the walls. The increase in $T_{\mathrm{lower\ cavity,\ bottom}}$ for fluff (Fig. 3d) was particularly slow due to the poor low-temperature

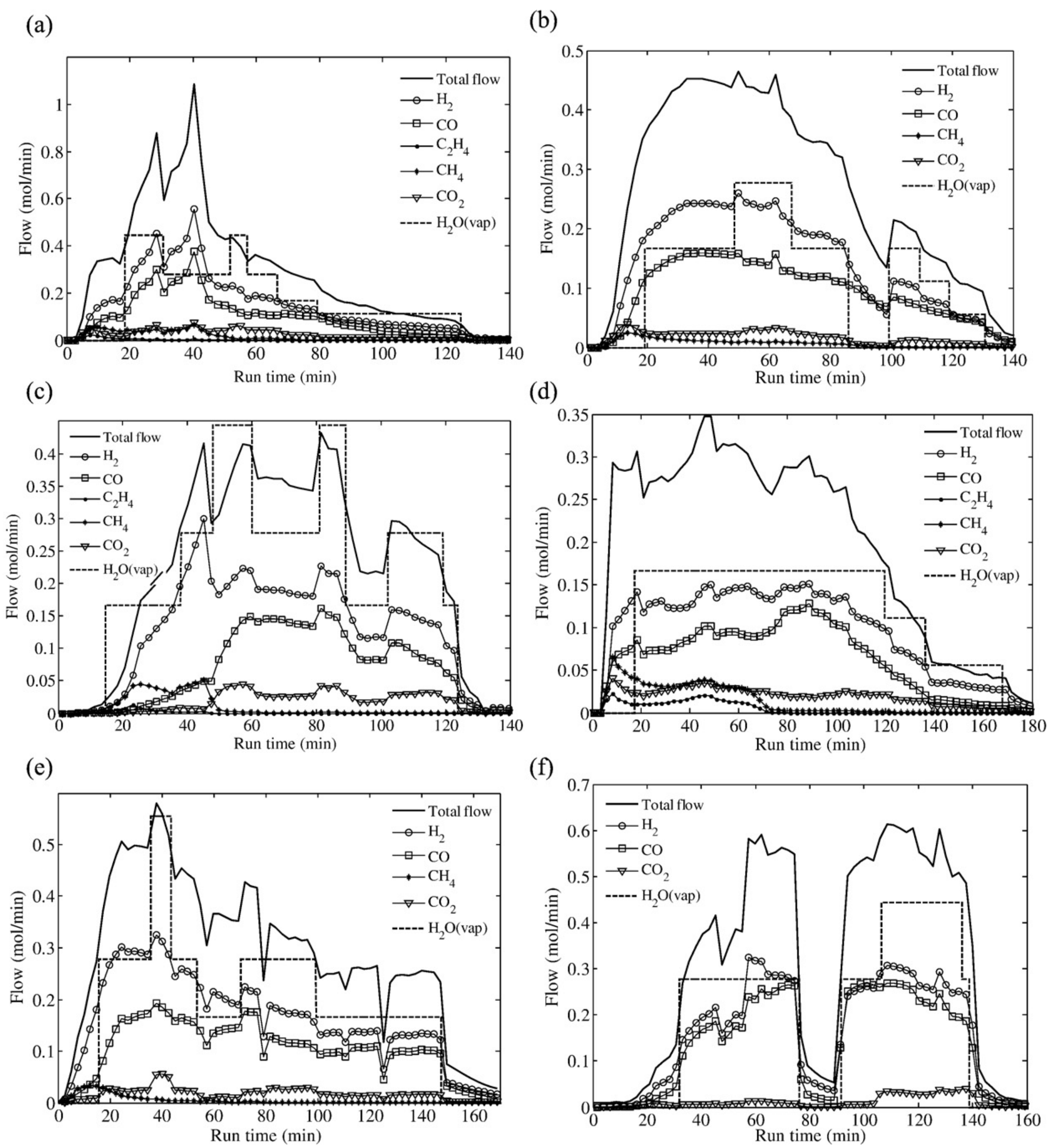

Fig. 4. Experimentally measured molar flow rates of evolved gases and steam supplied during the solar steam-gasification of: (a) industrial sludge, (b) sewage sludge, (c) scrap tire powder, (d) fluff, (e) South African coal, and (f) beech charcoal.

conductive heat transfer caused by the high porosity of the packed bed. In contrast, $T_{\text{lower cavity, bottom}}$ for the low-porosity packed bed of scrap tire powder (Fig. 3c) responded much faster.

As T_{emitter} and $T_{\text{lower cavity, top}}$ reached approximately steady-state values, less energy was required to account for thermal inertia and for the endothermic reaction of the shrinking packed bed. Both concurrent effects served to decrease the radiative power needed to maintain a given T_{emitter}. At the end of each experimental run, shut off of the HFSS was followed by a rapid drop in all temperatures owing to re-radiation losses through the aperture and conduction losses through the reactor walls.

Three reaction phases for the temperature profile of $T_{\text{lower cavity, bottom}}$ are indicated in Fig. 3a–f. Their description is exemplified for Fig. 3c. Phase 1 (between 0 and 50 min): water was removed at below 373 K. Devolatilization proceeded in the 400–800 K range, which caused a rapid reduction in bed depth. Because devolatilization is associated with a much lower endothermic enthalpy change than that for steam-gasification [24], the deep region of the bed saw no significant heat consumption and the temperature rose strongly aided by conductive heat transfer through the side walls. Phase 2 (between 50 and 110 min): $T_{\text{lower cavity, bottom}}$ rose above 950 K and was sufficient for the onset of important, strongly endothermic gasification reactions. Additionally, the bed shrink rate decreased compared to phase 1 due to slower reaction rates of gasification than those for pyrolysis. The curve of $T_{\text{lower cavity, bottom}}$ flattened in response. The reaction rate was limited by heat transfer through the packed bed characterized by a transient ablation regime in which the rate of heat transfer—predominantly by radiation—to the top layer of the packed bed undergoing endothermic gasification proceeded faster than the rate of heat transfer—predominantly by effective conduction—to the depth of the packed bed [19,22]. Phase 3 (between 110 min and end of run): the reactable mass was largely consumed, leaving ash which decreased the reaction rate and correspondingly the heat sink. Improved thermal conductivity supported by radiative heat transfer within the now shallow, high-temperature, packed bed served to drive a faster increase in $T_{\text{lower cavity, bottom}}$. The temperature profiles of $T_{\text{lower cavity, bottom}}$ in each reaction phase vary with the particular heat transfer properties and the reaction rates associated with each feedstock. Temperature flattening associated with phase 2 is virtually impossible to identify for industrial sludge, sewage sludge, and fluff due to the very low fixed carbon contents and correspondingly low fixed carbon gasification rates. Conversely, due to high fixed carbon contents, phase 2 is very pronounced for the South African coal and beech charcoal after the first steam interruption. No significant temperature increase is shown in phase 3 for industrial and sewage sludges due to the large inert ash layer which served to thermally insulate the bottom of the bed. The merging of the curves $T_{\text{lower cavity, bottom}}$ and $T_{\text{lower cavity, top}}$ in phase 3 for fluff indicates the complete conversion of the feedstock, with the remaining ash layer not impeding temperature equalization. For South African coal and beech charcoal, phase 3 is not indicated because the reactable mass was not depleted.

The corresponding measured gas evolution for the six feedstocks undergoing steam-gasification is shown in Fig. 4 along with the supplied steam molar flow rate. Gases with molar flow rates of less than 0.01 mol/min are omitted from the plots. Devolatilization reactions during the initial rapid heating phase up to 40 min are verified by the evolution of CH_4 and C_2H_4. As expected, fluff shows the most significant volatile release (Fig. 4d), with beech charcoal delivering virtually no freed volatiles (Fig. 4f). The clear end of CH_4 and C_2H_4 evolution marks the end of important devolatilization processes associated with bed temperatures exceeding 800 K. This is seen for industrial sludge (Fig. 4a) and scrap tire powder (Fig. 4c) with the end of CH_4 evolution at 50 min, and for fluff (Fig. 4d) with the end of CH_4 and C_2H_4 evolution at 70 min. For all feedstocks, CO and H_2 dominate the gas composition indicating a high-quality syngas, but their concentrations are strongly affected by temperature and the supply of water vapor. CO_2 evolution due to an increased water vapor supply is visible for scrap tire powder (Fig. 4c) at 45, 80, and 100 min and for beech charcoal at 110 min (Fig. 4f). The presence of CO and H_2 before the introduction of water vapor for feedstocks with high water content, i.e. industrial and sewage sludges and South African coal, points to water arising from drying in low-temperature bed regions supporting steam-gasification or cracking of released volatiles in high-temperature packed-bed regions.

Table 3
Performance indicators of the solar rector for the steam-gasification of carbonaceous feedstocks

Feedstock	Industrial sludge	Sewage sludge	Scrap tire powder	Fluff	South African coal	Beech charcoal
U (−)	1.07	1.16	0.83	0.69	1.25	1.30
η (%)	28	18	17.3	15.9	23.3	29
Packed-bed mass reduction (kg)	0.423	0.488	0.263	0.629	0.378	0.291
Average bed shrink rate (cm/h)	4.1	2.6	2.2	4.1	1.5	2.8
Packed-bed top surface temperature (K)	1490	1423	1470	1423	1470	1490

The upgrade factor and the solar-to-chemical energy conversion efficiency are defined as:

$$U = \frac{m_{\text{gas}} \cdot \text{LHV}_{\text{gas}}}{m_{\text{feedstock}} \cdot \text{LHV}_{\text{feedstock}}} \tag{1}$$

$$\eta = \frac{m_{\text{gas}} \cdot \text{LHV}_{\text{gas}}}{Q_{\text{solar}} + m_{\text{feedstock}} \cdot \text{LHV}_{\text{feedstock}}} \tag{2}$$

respectively, where Q_{solar} is the total solar energy delivered through the reactor's aperture over the duration of the experimental run, $m_{\text{feedstock}}$ is the feedstock mass which underwent gasification, and m_{gas} is the evolved gas mass with a composition determined by the GC, integrated over the duration of the experimental run. These and other performance indicators of the solar reactor and the process are shown in Table 3. The packed-bed mass reduction corresponds to gasification, devolatilization, and drying processes. Post-run analysis showed the remaining mass for industrial sludge, sewage sludge, and fluff to be composed of 100% ash with no carbon content. The runs for scrap tire powder, South African coal, and beech charcoal were stopped before all reactable mass was converted. U and η were calculated based on the *LHV* of the individual gas components at 298 K. Values of U greater than 1 indicate the successful storage of solar energy in chemical form and the upgrading of the calorific value of the fuel achieved with the solar gasification process. Values of U less than 1 are presumably due to deposits of liquid tars and carbonaceous solids within the tubing and filters which were not considered in the product $m_{\text{gas}} \cdot LHV_{\text{gas}}$ despite representing a significant portion of the calorific value of released products. Fluff, industrial and sewage sludges, and scrap tire powder produced significant solid and liquid deposits in the installation. The low volatile content of beech charcoal supported the production of high-purity syngas and yielded a high U as well as the highest η. The industrial sludge and fluff packed beds both shrank very rapidly owing to strong volatile release. The sewage sludge shrink rate was negatively influenced by packed-bed density changes over the course of the run due to agglomeration and sintering of the large quantities of ash.

5. Conclusions

The steam-gasification of complex and varying coal, biomass, and carbonaceous waste feedstocks into high-quality syngas has been experimentally demonstrated using a robust packed-bed solar reactor subjected to concentrated radiative energy. Heat transfer in the packed bed was characterized by an ablation regime, where the rate of radiative transfer to the endothermic reacting top surface was faster than the conductive heat transfer to the depth of the packed bed. Peak energy conversion efficiency of 29% and upgrade factor of 130% demonstrated the successful conversion and storage of solar energy in chemical form.

Nomenclature

LHV	low heating value, kJ/kg
m	mass, kg
Q	heat, kJ
T	absolute temperature, K
U	upgrade factor
η	energy conversion efficiency

Subscripts

bottom	bed bottom surface
emitter	emitter plate
lower cavity	lower cavity
top	bed top surface

Acknowledgements

We thank P. von Zedtwitz, S. Wepf and D. Ruch for the technical support during the experimental campaign at PSI's High-Flux Solar Simulator.

References

[1] P. Von Zedwitz, A. Steinfeld, The solar thermal gasification of coal—energy conversion efficiency and CO_2 mitigation potential, Energy 28 (2003) 441–456.
[2] D.W. Gregg, W.R. Aiman, H.H. Otsuki, C.B. Thorsness, Solar coal gasification, Solar Energy 24 (1980) 313–321.
[3] T. Kodama, T. Kondoh, T. Tamagawa, A. Funatoh, K-I. Shimizu, Y. Kitayama, Fluidized bed coal gasification with CO_2 under direct irradiation with concentrated visible light, Energy and Fuels 16 (2002) 1264–1270.
[4] D. Trommer, F. Noembrini, M. Fasciana, D. Rodriguez, A. Morales, M. Romero, A. Steinfeld, Hydrogen production by steam-gasification of petroleum coke using concentrated solar power—I. Thermodynamic and kinetic analyses, International Journal of Hydrogen Energy 30 (2005) 605–618.
[5] R. Mueller, P. Von Zedtwitz, A. Wokaun, A. Steinfeld, Kinetic investigation on steam gasification of charcoal under direct high-flux irradiation, Chemical Engineering Science 58 (2003) 5111–5119.
[6] A. Z'Graggen, P. Haueter, D. Trommer, M. Romero, J.C. de Jesus, A. Steinfeld, Hydrogen production by steam-gasification of petroleum coke using concentrated solar power—II Reactor design, testing and modeling, International Journal of Hydrogen Energy 31 (2006) 797–811.
[7] P. Von Zedwitz, A. Steinfeld, Steam-gasification of coal in a fluidized-bed/packed-bed reactor exposed to concentrated thermal radiation-modeling and experimental validation, Industrial & Engineering Chemistry Research 44 (2003) 3852–3861.
[8] A. Z'Graggen, P. Haueter, G. Maag, A. Vidal, M. Romero, A. Steinfeld, Hydrogen production by steam-gasification of petroleum coke using concentrated solar power—III. Reactor experimentation with slurry feeding, International Journal of Hydrogen Energy 32 (2007) 992–996.
[9] K.H. Van Heek, General aspects and engineering principles for technical application of coal gasification, in: J.L. Figuieiredo (Ed.), Carbon and Coal Gasification, NATO ASI Series, 1986, pp. 399–411.
[10] D.W. Gregg, R.W. Taylor, J.H. Campbell, J.R. Taylor, A. Cotton, Solar gasification of coal, activated carbon, coke and coal and biomass mixtures, Solar Energy 25 (1980) 353–364.
[11] M. Flechsenhar, C. Sasse, Solar gasification of biomass using oil shale and coal as candidate materials, Energy 8 (1995) 803–810.
[12] M. Morris, L. Waldheim, Energy recovery from solid waste fuels using advanced gasification technology, Waste Management 18 (1998) 557–564.
[13] P.D. Filippis, C. Borgianni, M. Paolucci, R. Pochetti, Prediction of syngas quality for two-stage gasification of selected waste feedstocks, Waste Management 24 (2004) 633–639.
[14] O. Senneca, R. Chirone, S. Masi, P. Salatino, A thermogravimetric study of nonfossil solid fuels. 1. Inert pyrolysis, Energy & Fuels 16 (2002) 653–660.
[15] B.A. Andersson, M. Lundberg, B. Heikne, U. Josefsson, Norrköping 75 MW CFB plant and biomass RDF combustion in fluidized-bed boilers, in: K. Sipilä, M. Rossi (Eds.), Proc. VTT Symposium—Power Production From Waste and Biomass IV: Advanced Concepts and Technologies, Espoo, Finland, 2002, pp. 185–210.
[16] S. Yagi, D. Kunii, Studies on effective thermal conductivities in packed beds, AIChE Journal 3 (1957) 373–381.
[17] A. Yogev, A. Kribus, M. Epstein, A. Kogan, Solar 'tower reflector' systems: a new approach for high-temperature solar plants, International Journal of Hydrogen Energy 23 (1997) 239–245.
[18] C. Wieckert, A. Meier, A. Steinfeld, Indirectly irradiated solar receiver reactors for high temperature thermochemical processes, Journal of Solar Energy Engineering 125 (2003) 121–123.
[19] B. Schaffner, A. Meier, D. Wuillemin, W. Hoffelner, A. Steinfeld, Recycling of hazardous solid waste material using high-temperature solar process heat. 2. Reactor design and experimentation, Environmental Science and Technology 37 (2003) 165–170.
[20] T. Osinga, G. Olalde, A. Steinfeld, Solar carbothermal reduction of ZnO: shrinking packed bed reactor modeling and experimental validation, Industrial & Engineering Chemistry Research 43 (2004) 7981–7988.
[21] C. Wieckert, U. Frommherz, S. Kräupl, E. Guillot, G. Olalde, M. Epstein, et al., A 300 kW solar chemical pilot plant for the carbothermic production of zinc, Journal of Solar Energy Engineering 129 (2007) 190–196.
[22] N. Piatkowski, A. Steinfeld, Solar driven coal gasification in a thermally irradiated packed bed reactor, Energy and Fuels 22 (2008) 2043–2052.
[23] J. Petrasch, P. Coray, A. Meier, M. Brack, P. Haeberling, D. Wuillemin, A. Steinfeld, A 50-kW 11,000-suns novel high-flux solar simulator based on an array of Xenon arc lamps, Journal of Solar Energy Engineering 129 (2007) 405–411.
[24] A.J. Lopez-Peinado, P.J.J. Tromp, J.A. Moulijn, Quantitative heat effects associated with pyrolysis of coals, ranging from anthracite to lignite, Fuel 68 (1989) 999–1004.